International Journal of Heat and Mass Transfer 254 (2026) 127709

Contents lists available at ScienceDirect

International Journal of Heat and Mass Transfer

journal homepage: www.elsevier.com/locate/ijhmt

Thermal conductivity of sugar alcohols: A molecular dynamics insight

Shukai Cheng [a,b,*], Donatas Surblys [b], Taku Ohara [b]

[a] Department of Finemechanics, Graduate School of Engineering, Tohoku University, Sendai 980-8579, Japan
[b] Institute of Fluid Science, Tohoku University, Sendai 980-8577, Japan

ARTICLE INFO

Keywords:
Molecular dynamics
Phase change materials
Sugar alcohols
Thermal conductivity

ABSTRACT

Sugar alcohols are widely studied and applied in various industrial fields as phase change materials (PCMs) for enhancing energy utilization and thermal management. Despite their inherent advantages, such as high latent heat and relatively higher thermal conductivity compared to other organic PCMs, the growing demand for improved applicational efficiency calls for a deeper understanding of their heat transfer mechanisms. Molecular-scale investigations can offer critical insights into these mechanisms, providing valuable guidance for the design of high-performance PCMs. In this study, equilibrium molecular dynamics (EMD) simulations were employed to calculate the thermal conductivity (TC) of representative sugar alcohols across a range of temperatures in both solid and liquid phases. The results reveal that TC decreases with increasing temperature with a pronounced drop observed during the solid–liquid phase transition. In the crystalline solid phase, TC exhibits noticeable anisotropy, which disappears upon transitioning into the liquid phase. Such anisotropy is also observed in the vibrational density of states, where the atomic vibrational modes in the solid state are different depending on the observed directions, indicating variation in interatomic interactions along different crystallographic directions. The decomposition analysis of TC shows that unbonded pairwise interactions contribute the most to the overall TC, with hydroxyl groups playing a particularly critical role. Further investigation into hydrogen bond (HB) reveals a strong correlation between the number of HBs and TC, while the orientation of HBs is closely linked to the observed anisotropy in TC. These findings offer new insights into the fundamental heat transfer mechanisms in sugar alcohols and are expected to serve as a theoretical foundation for the innovative design and optimization of future PCMs.

1. Introduction

With the growing energy demands of modern industry and increasing requirements for thermal management during equipment operation, researchers have shown immense interest in the development and innovation of phase change materials (PCMs) [1,2]. Relying on their latent heat storage characteristics, PCMs can not only address the issue of waste heat emission in industrial processes but can also store thermal energy for future reuse. Because of this, they have attracted widespread attention in various engineering fields. For example, in seasonal energy storage, solar energy collected in summer can be used during peak heating periods in winter, reducing the winter energy load and gaining broad applications in the construction sector [3]. In the current era of rapid development of new electric vehicles, PCMs with phase change occurring in the medium temperature range have been applied to battery thermal management systems [4]. They help to cool batteries and maintain optimal operating temperatures, thereby extending battery life. Furthermore, with the use of organic Rankine cycles (ORCs), the thermal energy stored by PCMs can be converted into electricity, broadening their application in diverse energy utilization scenarios [5].

Among the various types of PCMs, organic solid-liquid phase change materials are particularly well-suited for the aforementioned applications due to their stable chemical properties, non-toxicity, low volatility, and moderate phase change temperatures, along with minimal volume change during solid-liquid transitions [6]. However, despite the ability of organic PCMs to undergo phase changes within the moderate temperature range, their thermal conductivity is significantly lower than that of inorganic PCMs, hindering their efficient application [7]. Among organic PCMs, sugar alcohols have attracted increasing attention due to their unique molecular structure and abundant hydroxyl groups, which lead to higher latent heat and thermal conductivity in their pure form compared to other organic PCMs [8]. The hydroxyl groups in sugar alcohol molecules promote the formation of extensive hydrogen bond networks, which not only influence their phase change properties but

* Corresponding author.
E-mail address: cheng.shukai.p8@dc.tohoku.ac.jp (S. Cheng).

https://doi.org/10.1016/j.ijheatmasstransfer.2025.127709
Received 28 June 2025; Received in revised form 7 August 2025; Accepted 14 August 2025

also is expected to play a crucial role in thermal conduction [9]. In our previous work, we systematically analyzed the melting points and latent heat of sugar alcohols, providing insights into the mechanisms behind them [10]. These findings offer valuable reference points for tuning phase change temperatures and optimizing latent heat in sugar alcohol-based PCMs.

Nevertheless, even for sugar alcohols, their thermal conductivity still falls short of the efficiency requirements for practical heat utilization in industrial production, thereby limiting the full exploitation of their excellent latent heat storage properties. As such, enhancing the thermal conductivity of sugar alcohols is of great importance. Researchers have explored various approaches to improve the thermal conductivity of sugar alcohols, mainly by creating composite PCMs through the addition of other materials, such as nanoparticles or by embedding sugar alcohols into porous structures [11]. For instance, Srikanth Salyan et al. developed a novel composite PCM by adding nano copper oxide particles to mannitol, achieving a 25.2 % increase in thermal conductivity with just 0.5 wt !% of CuO nanoparticles [12]. His team also incorporated multi-walled carbon nanotubes into mannitol and observed that with 0.1 % and 0.5 % mass fractions of carbon nanotubes, the thermal conductivity of the composite increased by up to 7 % and 32 %, respectively [13]. Similarly, Liuhua Gao et al. enhanced erythritol's thermal conductivity by using expanded graphite as an additive, finding that the thermal conductivity increased continuously with the graphite content [14]. Xiang Qin et al. created a microframework composite PCM by combining erythritol with urea and carbon nanotubes within a wood-based cellulose matrix. They found that when the carbon nanotube mass fraction reached 1.5 %, the thermal conductivity of the composite reached a maximum 0.9832 W/(m·K), compare to 0.3865 W/(m·K) without carbon nanotube [15].

As demonstrated by these studies, researchers have achieved success in enhancing the thermal conductivity of PCMs through the addition of high-conductivity materials such as inorganic nanoparticles, carbon nanotubes, and graphene [16,17]. However, the mechanisms underlying these thermal conductivity improvements often remain unclear in experimental studies. Moreover, the intrinsic thermal conduction mechanisms of pure sugar alcohols themselves are still not fully understood. Without a thorough understanding of the fundamental heat transfer behavior in sugar alcohols, the design of new composite PCMs may lack theoretical guidance, potentially leading to longer time of development and unnecessary costs. Given the variety of molecular species and their potential application in composite PCMs, it is important to understand the heat conduction mechanism of sugar alcohols at a molecular level. Therefore, using computational simulations to analyze the heat transfer mechanisms of sugar alcohols is particularly valuable [18]. Since the sugar alcohol PCM matrix comprising the majority of the material by weight is typically sugar alcohol itself, uncovering the intrinsic thermal conduction behavior of sugar alcohols is crucial. This understanding will help guide the design of new PCM systems and yield more effective results.

In this study, we employ equilibrium molecular dynamics (EMD) simulations combined with the Green-Kubo method to predict the thermal conductivities of four sugar alcohols, which are commonly used as PCM matrices and with different number of hydroxyl groups: mannitol ($C_6H_{14}O_6$), arabinitol ($C_5H_{12}O_5$), erythritol ($C_4H_{10}O_4$) and glycerol ($C_3H_8O_3$), across different temperature ranges in both solid and liquid states. Firstly, the characteristics of thermal conductivity of these sugar alcohols are discussed. To better understand the heat transfer phenomena, we conduct the vibrational density of states analysis to examine atomic vibrational modes and also perform the decomposition analysis of the molecular mechanism that contributes thermal conductivity [19]. We analyze the variation of hydrogen bond numbers with temperature and phase change, further discuss the relationship between hydrogen bond orientation and thermal conductivity. At the end, the key findings of this study are summarized, emphasizing their relevance to understanding heat transfer in sugar alcohols. This study aims to shed light on the fundamental heat transfer mechanisms in sugar alcohols, providing a theoretical basis for the design of advanced PCMs.

2. Simulation details

2.1. Calculation setups

Building on our previous work [10], which demonstrated good agreement between simulated and experimental thermal properties of sugar alcohols with applying OPLS-AA force field [20], we continue to employ the OPLS-AA force field to model interatomic interactions, where the composition of this potential is shown in Eq. (1):

$$E_{\text{pot}} = E_{\text{bonds}} + E_{\text{angles}} + E_{\text{dihedrals}} + E_{\text{unbonded}}, \quad (1)$$

where the total potential energy E_{pot} consists of an intramolecular bonded part, including covalent bond interactions E_{bond}; angle bending interactions E_{angle}; torsion interactions E_{dihedral}, as well as an unbonded pairwise part E_{unbonded}, which includes van der Waals and Coulombic interactions. Detailed descriptions and parameters of the OPLS-AA force field can be found in Section S8 in Supporting Information. For unbonded interactions, a cut-off distance of 12 Å is employed for both van der Waals and short-range real-space Coulombic interactions. Long-range k-space Coulomb interactions are treated using the particle-particle particle-mesh (PPPM) method, with a precision of 1×10^{-6} [21]. To eliminate high-frequency vibrations in bonds containing hydrogen atoms, thereby improving calculational efficiency and enhancing the calculation accuracy of thermal conductivity, the SHAKE algorithm [22] is applied with a tolerance of 1×10^{-4} and a maximum of 100 iterations. The experimental crystal structure data [23–26] used in our earlier study is also adopted here to construct simulation systems, detailed information about the crystal unit cell can be found in Section S7 of Supporting Information. All simulations utilize three-dimensional periodic boundary conditions, and atomic motions are updated using the velocity Verlet algorithm [27] with an integration time step of 1 fs. All molecular dynamics simulations are conducted using the Large-scale Atomic/Molecular Massively Parallel Simulator (LAMMPS) [28], and Visual Molecular Dynamics (VMD) [29] software is used for molecular structure visualization.

2.2. System setups

Temperatures under which both solid and liquid sugar alcohols systems are built are shown in Table 1. Unless otherwise specified, all mentions of the "solid state" in this study refer specifically to the crystalline solid state. In order to calculate the thermal conductivity (TC) of sugar alcohols under various temperatures in solid and liquid phase, the initial configurations of all systems of four types of sugar alcohols are constructed based on the crystal unit cell structures obtained from experimental data [23–26], as mentioned in Section 2.1. In the constructed systems, the numbers of molecules for mannitol, arabinitol, erythritol, and glycerol are set to 540, 512, 432, and 480, respectively. Three-dimensional periodic boundary conditions are applied to all bulk systems to eliminate surface effects. For the solid-phase systems, an

Table 1
Temperatures used for the solid and liquid phase systems of sugar alcohols in this study. The highest temperature assigned to the solid-state simulations and the lowest temperature assigned to the liquid-state simulations are identical for each substance, correspond to the melting point of the respective sugar alcohols, as reported in our previous work [10].

Alcohols	Solid (K)				Liquid (K)			
Mannitol	300	350	400	456	456	500	550	600
Arabinitol	200	250	300	366	366	400	450	500
Erythritol	250	300	350	395	395	450	500	550
Glycerol	150	200	250	276	276	350	400	450

example is shown in Fig. 1, (detailed system configurational information of sugar alcohols can be found in Section S7 in Supporting Information) simulations start directly from the initial crystalline structures. A relaxation process is first performed under the NPT (isothermal and isobaric) dynamics at the targe temperature and 1 atm for 3 ns. This is followed by an additional 3 ns of relaxation under the NVT (isothermal and isochoric) dynamics at the same temperature, and then another 3 ns under the NVE (adiabatic and isochoric) dynamics to obtain the initial configuration for the sampling phase. The Nosé–Hoover [30] barostat and thermostat with 100 fs damping coefficient are applied for the relaxation processes. This equilibrated configuration is then used as the starting point for the equilibrium molecular dynamics (EMD) simulations, which are carried out under the NVE ensemble for 25 ns, during which data is collected. For liquid-phase system construction, an example is shown in Fig. 1, the crystalline systems of each sugar alcohol are used as the starting configuration. These are heated under 1 atm to fully melt the crystal structures within 3 ns. The maximum temperatures are set to 650 K for mannitol, 500 K for arabinitol, 600 K for erythritol and 450 K for glycerol to ensure complete transition to the liquid phase. After melting, the relaxation procedure mirrors that of the solid-phase systems: 3 ns in the NPT dynamics at the target temperature, follows by 3 ns in the NVT dynamics, and 3 ns in the NVE dynamics to obtain the initial configuration for the sampling phase. Subsequent production simulations are also conducted for 25 ns under the NVE ensemble with data collection. In the solid-phase simulations, a triclinic simulation box is employed, allowing independent adjustment of the box dimensions in all directions while the shear stress is fixed at 0. In contrast, for liquid-phase simulations, box length adjustments are coupled across all directions, which was enough to maintain isotropic pressure conditions. The schematic of simulation procedures can be found in Supporting Information.

2.3. Green-Kubo method

This study aims to investigate the mechanisms underlying the TC of various sugar alcohols across a range of temperatures and in both solid and liquid phases. Due to the intrinsic anisotropy arising from the molecular arrangements in molecular crystals under the solid phase, it is essential to measure the TC in multiple directions. In non-equilibrium molecular dynamics (NEMD) simulations, directional thermal conductivities are typically obtained by constructing separate systems for each direction and applying temperature gradients accordingly. However, this approach is computationally expensive. To reduce the computational burden while enabling the simultaneous measurement of TC in multiple directions from a single simulation, we employed EMD simulations combined with the Green–Kubo method in this study. This method has been demonstrated to yield results equivalent to those from NEMD in previous comparative studies [31]. The Green–Kubo method is based on the fluctuation–dissipation theorem [32] and evaluates the heat transport properties of a system in equilibrium. The core idea involves computing the time correlation of the instantaneous heat flux, as expressed in right term of Eq. (2):

$$\lambda_q = \frac{V}{k_B T^2} \int_0^\infty \langle \mathbf{J}_q(t) \otimes \mathbf{J}_q(0) \rangle dt, \tag{2}$$

where V, T are the systematic volume and temperature, respectively, k_B is Boltzmann constant, $\mathbf{J}_q(0)$ represents the total heat flux vector at time step 0, $\mathbf{J}_q(\mathrm{t})$ is the heat flux vector at time step t. With three systematic axes: x, y and z, tensor product operator $\otimes$ yields nine correlation series. By integrating those correlation series over time, one obtains the TC tensor λ_q. While in theory the integral eventually converges, due to numerical efficiency, we selected an integration window of 25 ps, with a sampling frequency of $dt = 5$ fs for the integration, with the detailed reason and description provided in the Supporting Information (Section S1). The calculated TC tensor consists of three diagonal elements corresponding to the x-, y-, and z-directional components, and six off-diagonal elements. However, the off-diagonal components are typically negligible (See Section S2 in Supporting Information), therefore, in this study, we focus only on the diagonal elements, which represent the thermal conductivities along the x, y, and z axes. An example of the crystal configurations aligned along these directions is shown in Fig. 2. In EMD simulations, the system remains in equilibrium and only exhibits fluctuations in heat flux. TC is derived from the method described above. The contribution of individual components (e.g., bond, angle, dihedral, unbonded interactions) to the overall TC is obtained by integrating the correlation between each partial heat flux and the total heat flux, as shown in Eq. (3) [33]:

$$\lambda_X = \frac{V}{k_B T^2} \int_0^\infty \langle \mathbf{J}_X(\mathrm{t}) \otimes \mathbf{J}_q(0) \rangle dt, \tag{3}$$

here, $\mathbf{J}_X(\mathrm{t})$ represents the partial heat flux (X can be e.g., bond, angle, dihedral, unbonded interactions) vector at time step t. The partial TC tensor λ_X is subsequently obtained to elucidate the individual contributions to overall heat conduction. And the partial TC tensors and the total TC tensor have the following relationship:

$$\lambda_q = \lambda_{\text{kinetic}} + \lambda_{\text{potential}} + \lambda_{\text{bond}} + \lambda_{\text{angle}} + \lambda_{\text{dihedral}} + \lambda_{\text{unbonded}} + \lambda_{\text{constrain}} \tag{4}$$

where the first two terms λ_{kinetic} and $\lambda_{\text{potential}}$ in the right part are atomic transport terms from kinetic energy and potential energy, respectively. The following four terms correspond to the interatomic interactions described in Eq. (1). The last term is from the constraint applied to the bond length connecting with hydrogen atoms, which is introduced in Section 2.1.

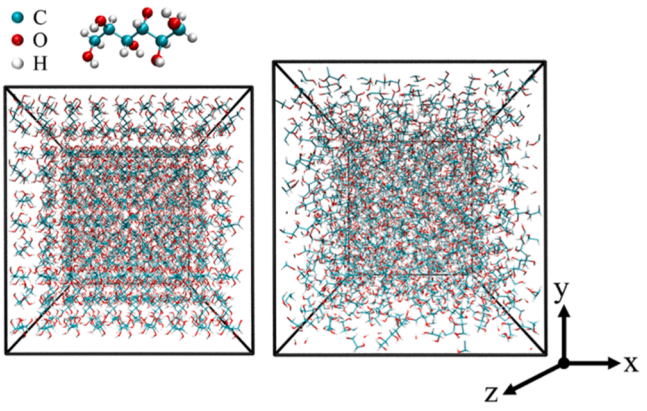

Fig. 1. Mannitol equilibrium molecular dynamics (EMD) simulation systems: the left panel is a crystal solid model at 300 K; the right panel is a liquid model at 600 K. A color-coded representation of a single mannitol molecule is provided in the top left.

2.4. Vibrational density of states

Via molecular dynamics, it is well understood that heat conduction in materials generally consists of two mechanisms: energy transport and interatomic interactions. Among these, vibrational motion is the most direct manifestation of interatomic interactions. In non-metallic solids, heat conduction occurs primarily through lattice vibrations, which can be described in terms of quantized vibrational modes known as phonons [34]. Phonon-based models have been extensively used to understand thermal transport in solids and have also shown some success when extended to liquids [35]. Vibrational density of states (VDOS) analysis provides valuable insight into the vibrational modes contributing to heat transfer and has been widely employed in relative studies [36]. As a

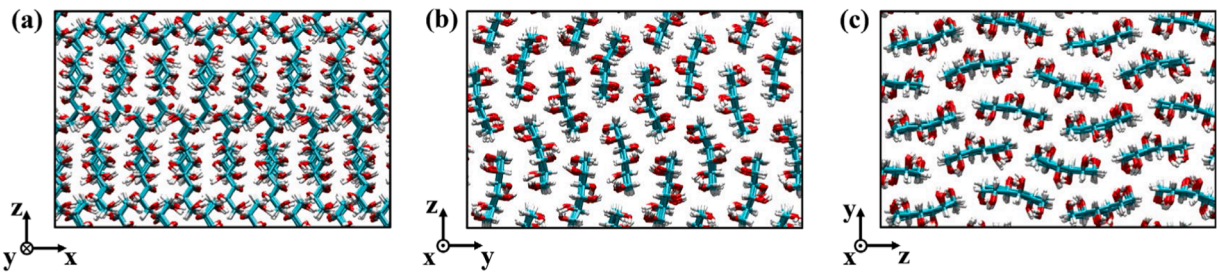

Fig. 2. Snapshots of mannitol crystalline configurations along x-, y- and z- directions at 300 K: (a) x direction; (b) y direction; (c) z direction.

commonly used method in molecular dynamics simulations, VDOS can be obtained by performing the Fourier transform of the velocity auto-correlation function (VACF) of atoms, as described by the following equation [37]:

$$V_I(\omega) = \frac{1}{\sqrt{2\pi}} \int_0^\infty m_i \langle \boldsymbol{v}_i(t) \cdot \boldsymbol{v}_i(0) \rangle e^{-i\omega t}\, dt, \tag{5}$$

where m_i is the mass of atom i, $\boldsymbol{v}_i(t)$ denotes the velocity of atom i in atom group I at time step t, ω is the angular frequency, and $V_I(\omega)$ represents the vibrational density of states of atom group I.

3. Results and discussion

3.1. Characteristics of thermal conductivity

Using the Green-Kubo method described in Section 2.3, we first calculated the thermal conductivities of four sugar alcohols along the x, y, and z directions across various temperatures in both solid and liquid states. In experimental measurements, the TC of a crystalline solid is typically reported as a single value. This is because most real-world crystals are polycrystalline unless specially prepared, which averages out anisotropy and results in macroscopically isotropic behavior. In contrast, molecular dynamics (MD) simulations often model idealized single crystals, which can exhibit pronounced anisotropy. Therefore, when comparing our simulation results with experimental data, we report the directional average of the TC along the x, y, and z axes as the effective value, as indicated by the black lines in Fig. 3. In the experimental studies available to us [8,38,39], data for thermal conductivities of sugar alcohols across multiple temperatures was not accessible. Thus, we compare our simulation results with the available experimental data at selected temperatures. As shown in Table 2, for instance, the TC of mannitol at 23 °C (296 K) is reported as 0.83 W/m·K, which agrees well with our simulation result of 0.83 ± 0.02 W/m·K at 300 K in solid state. In the liquid state, the experimental TC of mannitol at 178 °C (451 K) is reported as 0.37 W/m·K, while our simulation yields 0.41 ± 0.01 W/m·K at 455 K. Overall, the agreement between the simulation and the experimental values is reasonably good with matching range of 84 % to 99 %, supporting the suitability of the OPLS-AA force field in studying the TC of sugar alcohols [40].

As expected, as shown in Fig. 3, all sugar alcohols exhibit a general trend of decreasing TC with increasing temperature. In the solid crystalline state, thermal conductivities are significantly higher than in the liquid state. Moreover, the crystalline state shows clear anisotropy in TC

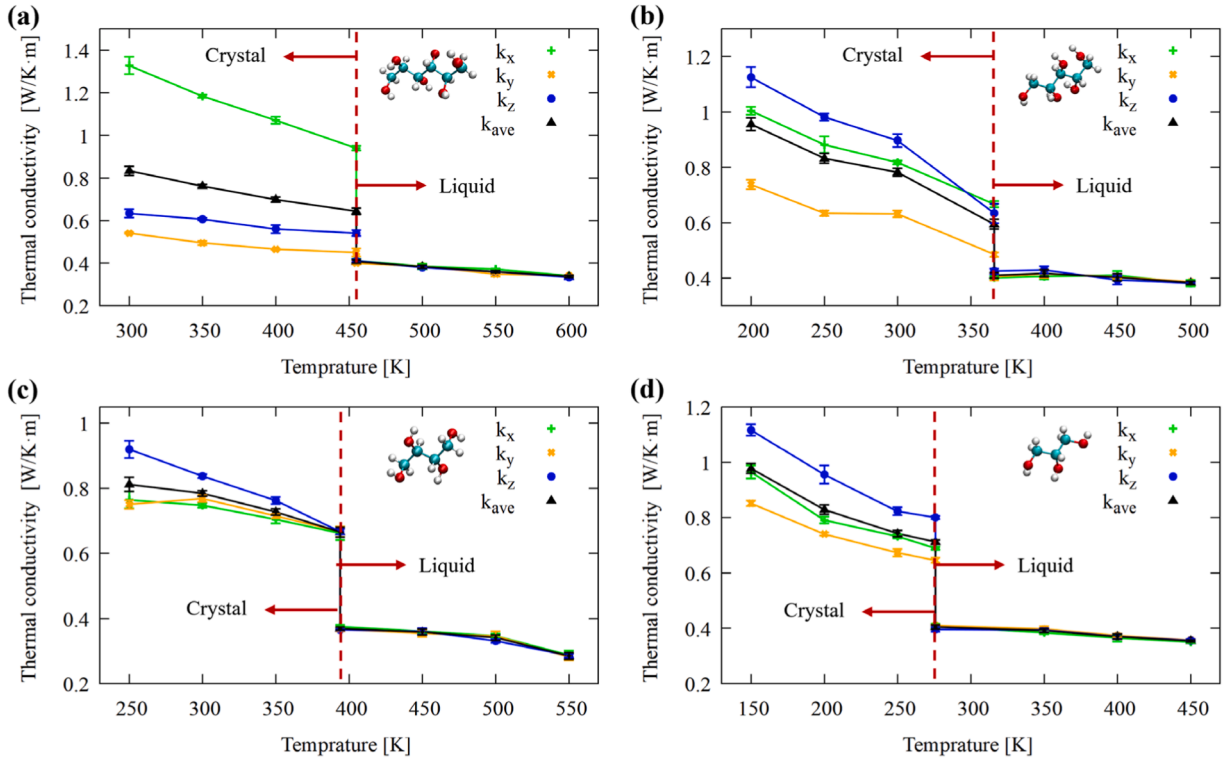

Fig. 3. Thermal conductivity of sugar alcohols at various temperatures in solid and liquid phases: (a) mannitol; (b) arabinitol; (c) erythritol; (d) glycerol. The red dashed line marks the separation between solid and liquid phases.

Table 2
Calculated thermal conductivity (TC) values obtained in this study, compared with experimental results. The second and third columns show the calculated TC of sugar alcohols in the solid and liquid states, respectively. The fourth and fifth columns present corresponding experimental TC data in the solid and liquid states. In each cell, the value on the left (with its statistical standard error in parentheses) represents the TC (e.g., 0.83(2) indicates 0.83 ± 0.02). The number on the right, enclosed in parentheses, indicates the temperature at which the TC was measured.

Alcohols	k_{ave} [W/K·m]	k_{ave} [W/K·m]	Experiment [8,38,39]	
Mannitol	0.83(2) (300 K)	0.41(1) (455 K)	0.83 (296 K)	0.37 (451 K)
Arabinitol	0.78(1) (300 K)	0.42(1) (400 K)	0.93 (298 K)	N/A
Erythritol	0.78(1) (300 K)	0.37(1) (394 K)	0.77 (298 K)	0.34 (398 K)
Glycerol	0.74(2) (250 K)	0.39(1) (350 K)	0.88 (250 K)	0.29 (313 K)

across different directions, with mannitol exhibiting the most pronounced anisotropy. For example, as seen in Fig. 3(a), at 300 K, mannitol has a TC of 1.33 W/m·K in the x direction, 0.54 W/m·K in the y direction, and 0.63 W/m·K in the z direction, more than twice the conductivity in x compared to the other directions. Similarly, for arabinitol and glycerol, three different values are observed along the x, y, and z directions. Erythritol (Fig. 3(c)) at 250 K shows nearly identical conductivities 0.76 W/m·K and 0.75 W/m·K in the x and y directions, respectively, with a higher value in the z direction, 0.92 W/m·K. Such near-equality in two directions was not observed in the other substances. Importantly, this directional anisotropy in the crystalline phase persists across the entire temperature range studied, although the degree of anisotropy diminishes with increasing temperature. The relative magnitude of TC in the x, y, and z directions remains mostly constant regardless of temperature.

The origin of this anisotropy lies in the intrinsic structural characteristics of the crystal lattice [41]. Therefore, the observed directional dependence of TC in the solid state is closely linked to the molecular crystal structures of sugar alcohols. As discussed earlier, while anisotropy is prominent in the crystalline state at lower temperatures, it disappears upon melting. This is evident in the liquid-phase regions of Fig. 3, where the thermal conductivities along x, y, and z converge to same values. We attribute this to the destruction of the ordered crystal structure upon melting, resulting in isotropic behavior and equal thermal conductivities in all directions. A more detailed analysis and explanation will be provided in the following sections.

3.2. Vibration density of state (VDOS) analysis

It is well understood that interatomic interactions are one of the primary underlying mechanisms of heat conduction, and these interactions are most directly manifested through atomic vibrations. Therefore, in this section, we analyze the vibrational behavior of different atoms within sugar alcohol molecules in both solid and liquid states, as has been used in previous literature [42], to provide a perspective on their heat transfer mechanisms. By extracting and comparing the VDOS which was introduced in Section 2.4, we aim to shed light on the microscopic origins of TC in these materials. Fig. 4 presents the VDOS of mannitol in both the solid state at 300 K and the liquid state at 600 K. The analysis was carried out for four distinct types of atoms present in sugar alcohol: carbon atoms, oxygen atoms, hydrogen atoms bonded to carbon, and hydrogen atoms bonded to oxygen (the two types of hydrogen atoms were treated separately). Furthermore, in order to take a closer look at the directional vibrational modes, the vibrational components along the x, y, and z directions were analyzed independently for each atomic type. As shown in Fig. 4(a), in the solid state, the vibrational modes of oxygen atoms are primarily concentrated in the low-frequency region below 20 THz. While carbon atoms also exhibit vibrational modes in this low-frequency range, they additionally show distinct peaks at higher frequencies. In contrast, both types of hydrogen atoms display relatively fewer vibrational modes in the low-frequency region, but they exhibit significant peak intensities in the relatively higher-frequency range between 20 and 40 THz. The spectral intensity in the low-frequency region primarily arises from unbonded interactions, as noted in previous study [43]. Based on this understanding, it can be inferred that the interactions involving oxygen atoms, which only exist in hydroxyl groups, play a major role in the heat conduction process caused by unbonded interatomic interactions of sugar alcohols. In other words, it is expected that hydrogen-bond-related heat transfer is primarily mediated by vibrational energy exchange between oxygen atoms. A more detailed discussion will be presented in the latter sections based on TC decomposition and hydrogen bond analysis. Fig. 4(b–d) further reveal the direction-dependent vibrational behavior of mannitol in the solid state. Notably, the oxygen atoms exhibit broader low-frequency vibrational distributions along the x and z directions compared to the y direction. Directional differences are also evident for the other atomic types, indicating a pronounced anisotropy in the vibrational characteristics, consequently, in the heat transfer mechanisms of crystalline mannitol. In contrast, the VDOS of liquid-state mannitol, shown in Fig. 4(e–h), exhibits a high degree of isotropy. The vibrational distributions along the x, y, and z directions are nearly identical and coincide with the total VDOS, indicating that directional differences in heat transfer vanish upon melting. This isotropic behavior in the liquid phase also suggests that the structural order responsible for anisotropic thermal transport in the crystalline state is lost due to melting [44].

The other three sugar alcohols (erythritol, glycerol, and arabinitol) exhibit similar VDOS trends as mannitol in both solid and liquid phases. Specifically, oxygen atoms consistently dominate the low-frequency region, and directional anisotropy is observed in the solid phase but disappears in the liquid phase. Due to the similarity in trends and limitations of figure space, detailed VDOS analyses for these sugar alcohols are provided in the Supporting Information (Section S3).

3.3. Decomposition of thermal conductivity

To gain deeper insight into the heat conduction mechanisms of sugar alcohols in different phases, and to identify the origins of the observed anisotropy in the crystalline state, we performed the decomposition analysis of TC [19] based on the types of interatomic interactions. Specifically, we classified and compared the heat flux contributions according to various interaction types between atoms.

As shown in Fig. 5, the decomposed TC components of four sugar alcohols in both the solid and liquid phases are presented (only the results at selected temperatures are shown here for comparison; for the complete dataset, please refer to Supporting Information Section S4). In general, for all sugar alcohols and under both phases, unbonded pairwise interaction consistently makes the largest contribution to the total TC, exceeding any other individual component. This indicates that unbonded interaction between atoms dominates thermal transport in sugar alcohols. Additionally, the bond and angle interactions also play significant roles, suggesting that the stretching vibrations of covalent bonds and bending motions of molecular bond angles contribute noticeably to thermal conduction. On the other hand, the contribution of the dihedral interaction is negligible across all sugar alcohols and in both phases, leading to the conclusion that torsional motions have little influence on the thermal transport of these molecules. Besides the interatomic interactions, we also examined the transport term, which consists of potential and kinetic energy contributions. Although the magnitudes of the transport terms are comparable between solid and liquid phases, their relative contributions differ. In the solid phase, the transport term contributes only marginally to the overall TC, whereas in the liquid phase, its proportion becomes larger. The kinetic contribution is particularly small in the solid phase, and the transport term is dominated by the potential part. This behavior arises because molecular motion in solids is largely confined to vibrations around fixed equilibrium positions. In contrast, in the liquid phase, molecules gain

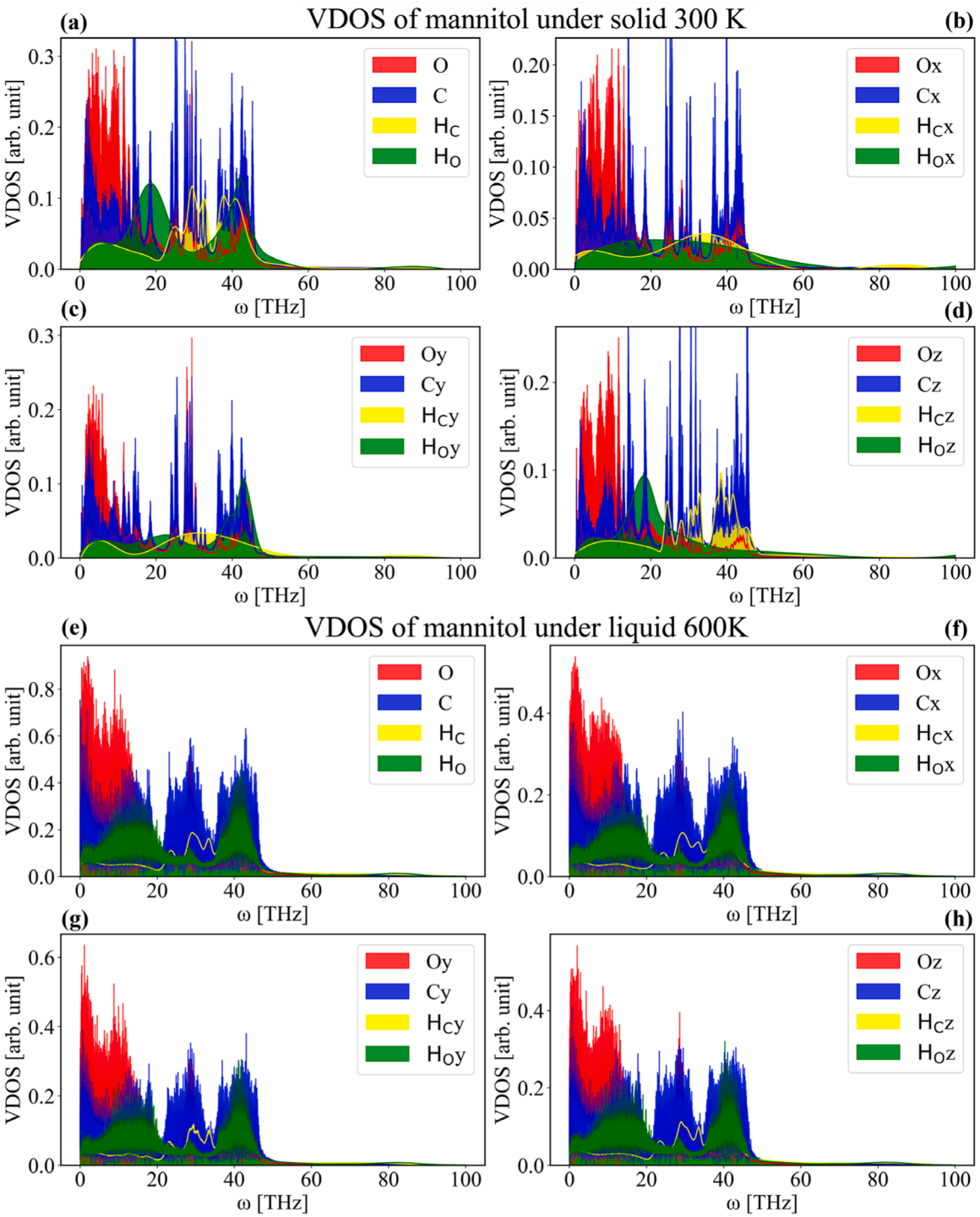

Fig. 4. Vibrational density of states (VDOS) for four atoms of mannitol in solid and liquid phases. (a) Total VDOS of mannitol at 300 K in the solid state; (c–d) directional VDOS along the x-, y-, and z-axes at 300 K in the solid state; (e) total VDOS of mannitol at 600 K in the liquid state; (f–h) directional VDOS along the x-, y-, and z-axes at 600 K in the liquid state.

additional degrees of freedom and exhibit translational motion. As a result, the absolute values of kinetic contribution increase in the liquid phase, even though the potential contribution still remains dominant. Furthermore (please see the Section S4 of Supporting Information), with increasing temperature, either within the same phase or during the solid-to-liquid transition, each component of the TC tends to decrease, which can be explained by intensified phonon-phonon scattering that reduces lattice TC [45], and by the loss of crystal order and transition to disordered molecular motion during the solid-liquid phase change, which further suppress heat conduction. While the proportions of each component remain relatively stable at different temperatures within the same phase, more dramatic decreases and vanishment of directional differences are observed during phase transitions. Notably, the pairwise interaction term (representing unbonded interactions) shows a particularly sharp reduction upon melting, accompanied by a sharp decrease in density (as shown in Section S6 in Supporting Information). This increase in molecular spacing suggests that an efficient heat conduction pathway is disrupted due to the loss of the crystalline structure.

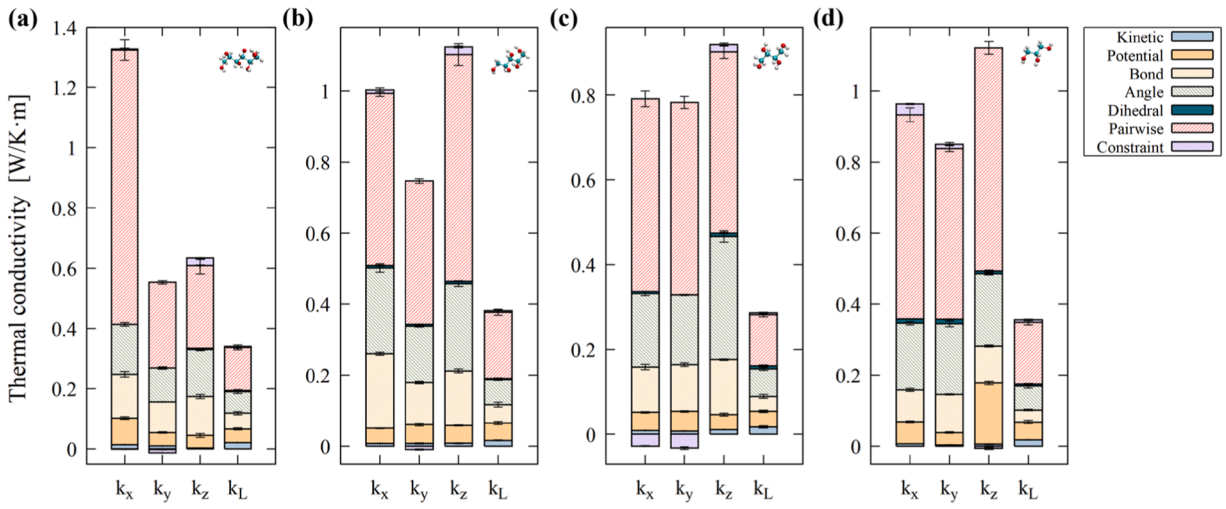

Fig. 5. Thermal conductivity of sugar alcohols decomposd into kinetic, potential, bond, angle, dihedral, pairwise and constraint components: (a) mannitol, k_x, k_y, k_z is under 300 K in solid state, k_L is under 600 K in liquid state; (b) arabinitol, k_x, k_y, k_z is under 200 K in solid state, k_L is under 500 K in liquid state; (c) erythritol, k_x, k_y, k_z is under 250 K in solid state, k_L is under 550 K in liquid state; (d) glycerol, k_x, k_y, k_z is under 150 K in solid state, k_L is under 450 K in liquid state. The thermal conductivity in the liquid state is isotropic, and thus only a single representative result is presented.

Additionally, directional differences in TC disappear in the liquid phase, indicating a clear change in heat transfer mechanisms across the phase boundary.

The above decomposition results clearly demonstrate that the majority of heat transport in sugar alcohols, regardless of phase, is governed by interatomic interactions. Next, we focus on individual compounds. For mannitol, which exhibits the most pronounced anisotropy in TC (Fig. 5(a)), the TC along the x-direction is significantly higher than that in the y- and z-directions. This is primarily due to a much greater contribution from pairwise interactions (Coulombic and van der Waals) along the x-direction, where they account for approximately 68 % of the total conductivity. While the pairwise interaction contributions in the other two directions are similar and much smaller than in the x-direction, they still constitute the dominant channel for thermal transport in those directions. For arabinitol, shown in Fig. 5(b), the highest TC in the z-direction (compared to x and y) also stems from a larger pairwise interaction contribution in that direction. Additionally, both angle and bond contributions are higher along the x- and z-directions than along y, reinforcing the directional preference of heat transport. In the case of erythritol (Fig. 5(c)), thermal conductivities in the x- and y-directions are nearly identical, and the z-direction conductivity is only slightly higher. The decomposition of TC shows that while the z-direction has slightly smaller pairwise interaction contributions compared to x and y, it compensates with a higher angle interaction contribution. This results in slightly higher TC in the z-direction. The symmetric crystalline structure of erythritol in the x- and y-directions explains the nearly identical thermal conductivities and mechanisms in these directions (see Section S7 in Supporting Information), as well as the relatively low anisotropy in its thermal transport behavior. Finally, for glycerol (Fig. 5(d)), the pairwise interaction contribution is slightly higher in the z-direction than in the x-direction, which in turn is slightly higher than in the y-direction. Additionally, the potential component of the transport term contributes notably to the heat flux in the z-direction. The exact reason remains unclear, as no noticeable displacement is observed along this axis, though it may be related to crystal anisotropy or greater vibrational amplitudes of the lattice in that direction.

As a further step in the analysis, motivated by mannitol's pronounced anisotropy, we decomposed the pairwise interaction term of mannitol in greater detail. First, we separated the van der Waals and Coulombic components. As shown in Fig. 6(a), in all cases, including the x, y, and z directions in the solid phase and the isotropic liquid phase, the contribution from van der Waals interactions consistently exceeds that

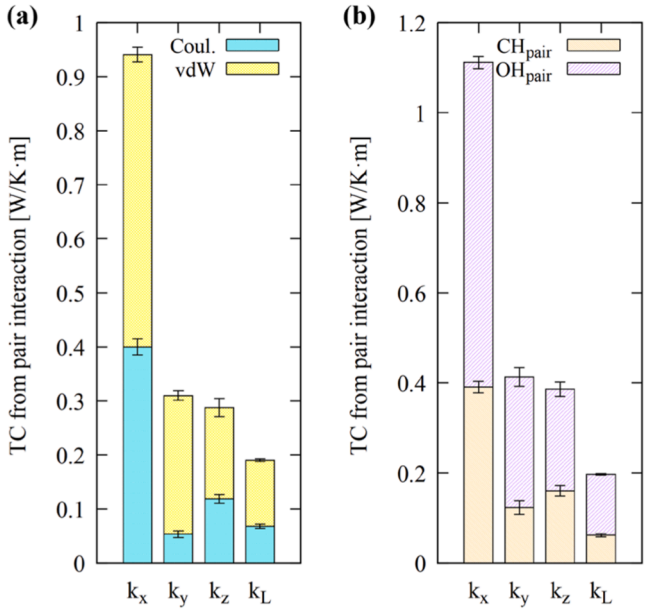

Fig. 6. Further decompositions of unbonded pairwise thermal conductivity contribution of mannitol: (a) contribution of Coulombic interaction and van der Waals interactions; (b) contribution from CH groups and OH groups (short-range contributions under cut-off distance 18 Å). In both figures, k_x, k_y, k_z is under 300 K in solid state, k_L is under 600 K in liquid state. The thermal conductivity in the liquid state is isotropic, and thus only a single representative result is presented.

of Coulombic interactions. This underscores the critical role of van der Waals forces in the thermal transport of sugar alcohols. Given that sugar alcohols contain abundant OH groups, whose interactions are governed primarily by van der Waals and Coulombic forces, we also divided the pairwise term into contributions from OH–OH and CH–CH interactions. As illustrated in Fig. 6(b), the results consistently show that OH–OH interactions dominate the thermal transport across all directions and phases. This finding suggests that hydroxyl groups play a crucial role in determining the TC of sugar alcohols and may also be key contributors to the anisotropic heat transport observed in the crystalline phase. Combining the insights from the VDOS analysis, it is highly suggested

that heat is primarily exchanged through the vibrations of oxygen atoms in hydroxyl groups within the hydrogen-bond network. It should be also noted that the total values of CH- and OH-groups contributions shown in this decomposition differ slightly from the total pairwise contributions. This discrepancy arises from the use of an approximation that includes only short-range Coulombic interactions, due to the difficulty of accurately handling long-range Coulombic effects. However, this does not affect the validity of the conclusions drawn above. A detailed explanation and discussion of this issue is provided in the Supporting Information Section S5.

3.4. Insight into heat conduction via hydrogen bonding

At the end of the previous section, we briefly mentioned the critical role of hydroxyl groups in the thermal transport behavior of sugar alcohols. In this section, we delve deeper into the role of hydrogen bonding in thermal conduction by analyzing the formation and orientation distribution of hydrogen bonds (HBs) in sugar alcohols. As shown in Fig. 7(a), we determined the presence of HBs based on the same criteria used in our previous work [10], and we employed the MDAnalysis toolkit [46] to carry out the HB analysis. Fig. 8 presents the average number of HBs per molecule for four sugar alcohols under different temperatures and phases (solid or liquid). Overall, it is evident that in both solid and liquid states, the number of HBs decreases linearly as the temperature increases [47]. Further investigation reveals that the hydrogen bond (HB) lifetime decreases with increasing temperature as well (see Section S9 in Supporting Information). This phenomenon has also been observed in an experimental studies using infrared spectroscopy, where hydrogen bonds weaken with increasing temperature [48]. This trend aligns with the TC results shown in Fig. 3, where the TC k_{ave} of sugar alcohols also decreases with increasing temperature. Additionally, at the melting point, a sharp drop in the number of HBs is observed due to the collapse of the crystal structure during the phase transition from solid to liquid. This sudden decrease in HBs corresponds to the steep decline in TC upon the solid-liquid transition, seen in Fig. 3. Based on these observations, we can confidently conclude that, for the same sugar alcohol, its TC at a given temperature and phase is highly correlated to the average number of HBs formed per molecule. In other words, a greater number of HBs per molecule generally leads to higher TC. Furthermore, by combining the VDOS analysis with insights from TC decomposition, both of which highlight the critical role of oxygen atoms in heat conduction, we conclude that vibrational energy exchange between oxygen atoms in hydroxyl groups through HBs constitutes the main mechanism of heat transfer in sugar alcohols. However, no clear correlation is observed when comparing different sugar alcohols (A brief comparison of the factors that may affect TC across different sugar alcohols is provided in Section S10 of the Supporting Information.). For example, in Fig. 8(b) and Fig. 8(d), arabinitol at 250 K forms significantly more HBs than glycerol at 150 K, yet glycerol exhibits higher TC at that temperature. We speculate that this discrepancy may stem from differences in the type and nature of HBs formed in each sugar alcohol. In addition to HB, other heat transfer pathways, such as intramolecular bonded interactions, may also vary due to differences in molecular structure, all of which could influence their contribution to heat transfer. As this work focuses on the general thermal transport mechanism rather than explaining conductivity differences among different sugar alcohols, we leave this issue for future investigation.

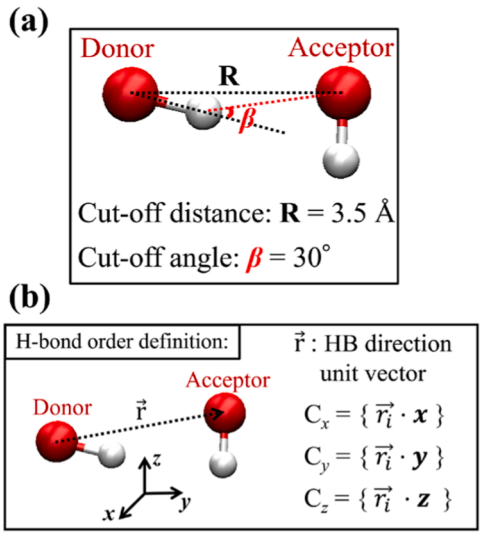

Fig. 7. (a) Geometrical hydrogen bond formation definition. (b) schematic of hydrogen bond order analysis: r_i is the unit vector of the i th hydrogen bond, and x, y, z are unit vectors along the respective Cartesian axes.

As shown schematically in Fig. 8, in the absence of external disturbances, such as electric field or external force, the number of HBs formed at a given temperature and phase remains relatively constant. A deeper question then arises: how do these HBs lead to TC anisotropy in solids and isotropy in liquids? As illustrated in Fig. 7(a), a HB is defined by a donor and acceptor oxygen atom pair that satisfies certain distance and angular conditions. Once formed, especially in the solid phase at lower temperatures, these HBs are relatively stable and only vibrate around their equilibrium positions. Consequently, HBs possess strong directionality, meaning that they may exhibit preferential alignment along specific spatial directions. To quantify the direction of a HB, as shown in Fig. 7(b), we define a vector pointing from the donor oxygen to the acceptor oxygen (HB direction unit vector), and we analyze its orientation relative to the x, y, and z coordinate axes. Specifically, we calculate the absolute value of the cosine of the angle between the HB direction vectors and each coordinate axis, with values ranging from 0 to 1. These absolute cosine values, denoted as C_x, C_y, and C_z, represent sets of values (not single values), as shown in Fig. 7(b) as well. We then apply a nonparametric method, kernel density estimation (KDE) [49] to approximate the probability density distribution of these sets over the range (0, 1). It should be noted that this method has a known limitation, as it may produce estimations of non-existent distributions outside the boundaries of the original dataset [50]. Nevertheless, the distribution within the main region is accurately captured. The orientation distributions of HBs for four sugar alcohols under solid and liquid phases are shown in Fig. 9. In general, sugar alcohols in the solid phase exhibit clear peaks in the cosine value distributions in each direction, with noticeable differences among the x, y, and z directions, indicating significant orientation preferences of HBs. In contrast, the cosine distributions in the liquid phase are relatively flat and uniform across all directions, suggesting that HB directionality disappears upon melting. This loss of orientation can be interpreted as one of the underlying reasons for the disappearance of TC anisotropy during the solid-to-liquid phase transition. Let us take a closer look at Fig. 9(a). For mannitol in the solid phase, the C_x values are mainly distributed between 0.8 and 1.0 (37° – 0°), C_z values fall between 0.3 and 0.6 (73° – 53°), and C_y values are mostly between 0 and 0.3 (90° – 73°), with a smaller portion between 0.8 and 1.0 (37° – 0°). A cosine value close to 1 implies a small angle (0°) between vectors, i.e., the HB direction is nearly parallel to that coordinate axis. Conversely, values near 0 indicate near-perpendicular (90°) orientation. Thus, Fig. 9(a) shows that most HBs in solid mannitol are highly aligned with the x direction, followed by the z direction, with the least alignment along y. This explains why mannitol exhibits the highest TC along x, and why the z-direction TC is slightly higher than that of the y direction. We propose that if most HBs are aligned along a certain direction, heat flow can more easily propagate through them, leading to higher TC in that direction. A similar trend is observed in Fig. 9(b) for arabinitol, where in the region with absolute cosine values above 0.5, the density follows the order $C_z > C_x > C_y$, consistent with the directional TC values $k_z > k_x > k_y$. As for erythritol (Fig. 9(c)), the distributions of C_x and C_y exhibit almost identical trends, suggesting a strong

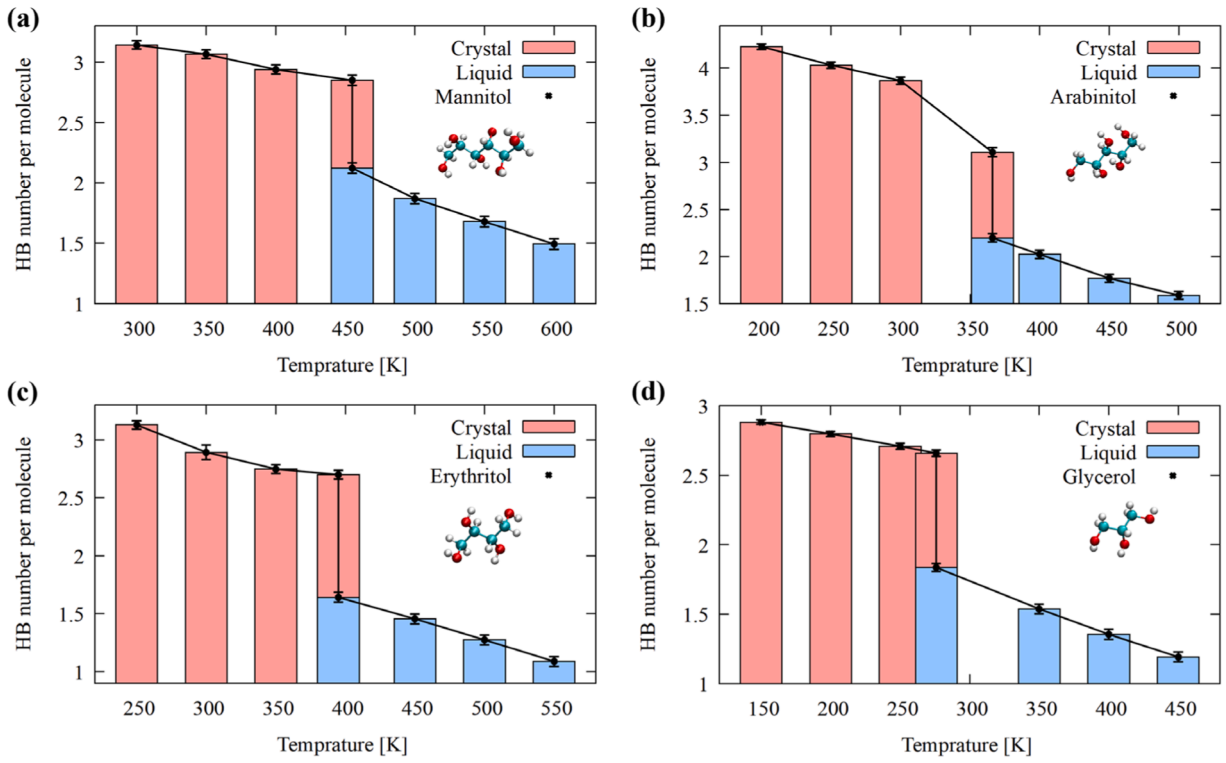

Fig. 8. Hydrogen bond number per molecule at various temperatures in solid or liquid phase: (a) mannitol; (b) arabinitol; (c) erythritol; (d) glycerol.

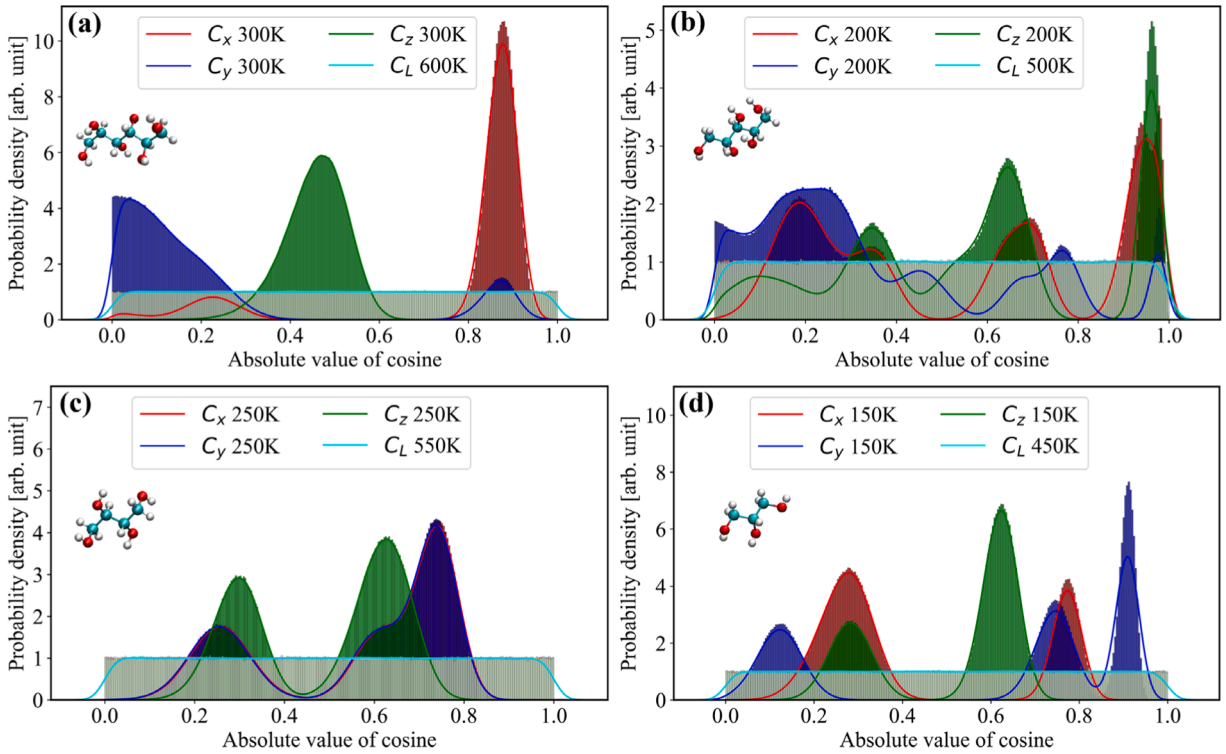

Fig. 9. Hydrogen bond order distributions fitted using kernel density estimation (KDE) in both solid and liquid phases. The enveloped histograms represent the original data distributions of C_x, C_y and C_z. The analyzed temperatures are indicated in the legends; lower temperatures correspond to the solid phase, while higher temperatures represent the liquid phase (labeled with the subscript "*L*"), which exhibits directional isotropy: (a) mannitol; (b) arabinitol; (c) erythritol; (d) glycerol.

correlation between the isotropic HB orientation in the xy plane, which can be attributed to the identical crystalline morphology along the x and y axes (as described in Section S7 in Supporting Information), and the thermal conductivities in the x and y directions are nearly the same. For glycerol, as shown in Fig. 9(d), the probability distribution of HB orientations appears rather disordered, with multiple peaks occurring in

the range above 0.5, and no clear relationship among C_x, C_y, and C_z. Although TC anisotropy can still be observed in the solid state of glycerol, we speculate that for sugar alcohols with shorter chain lengths and distinct crystalline structures in different directions (see Section S7 in Supporting Information), the influence of HB orientation on TC becomes weaker.

4. Conclusions

In this study, we conducted a comprehensive investigation of the thermal conductivity (TC) characteristics of four sugar alcohols: mannitol ($C_6H_{14}O_6$), arabinitol ($C_5H_{12}O_5$), erythritol ($C_4H_{10}O_4$) and glycerol ($C_3H_8O_3$), via molecular dynamics (MD) simulation. This research reveals fundamental rules governing heat conduction in sugar alcohol-based phase change materials (PCMs) and emphasizes the critical role of hydrogen bonding in determining thermal transport efficiency. The key findings and insights can be summarized as follows:

The TC of all studied sugar alcohols exhibited a monotonic decrease with increasing temperature in both solid and liquid phases. This behavior is consistent with the general understanding that increased molecular motion and disorder at higher temperatures hinder efficient phonon transport in solids, and the increase in thermal agitation disrupts coherent energy transfer pathways in liquids. A sharp drop in TC was observed during the phase change, which is due to the loss of long-range crystalline order and the breakdown of structured heat transfer pathways during the solid-to-liquid transition. In the solid phase, thermal conductivity exhibited pronounced anisotropy, with distinct differences in the x-, y-, and z-axis directions. This anisotropy disappeared in the liquid phase, where molecular disorder and isotropic mobility led to same TC values in all directions. Vibrational density of states (VDOS) analysis suggested that oxygen atoms played an important role in heat conduction. Also, directional differences were shown in vibrational modes of solid sugar alcohols, indicating the directional anisotropy in interatomic interactions. Based on different types of interactions, TC decomposition analysis revealed that the majority of heat conduction occurs via unbonded pairwise interactions (van der Waals and Coulombic) rather than bonded atomic vibrations. Further decomposition of mannitol TC demonstrated that in unbonded pairwise interactions, particularly those associated with hydroxyl groups, contribute most to heat conduction. Detailed hydrogen bond (HB) analysis showed that the number of hydrogen bonds per molecule decreased linearly with increasing temperature and exhibited a sudden drop at the solid-liquid transition, paralleling the trend of TC. A clear positive correlation between the average HB number and thermal conductivity was established for each sugar alcohol across different temperatures and phases. However, this correlation did not hold strictly across different species (e.g., arabinitol has more hydrogen bonds than glycerol, but its thermal conductivity is not necessarily higher than that of glycerol), suggesting that not just the number, but also the type, strength, and directionality of hydrogen bonds influence TC. Orientation distribution analysis of HB revealed significant alignment in specific directions in the solid phase, which corresponded closely to the directions with higher thermal conductivity. For example, in mannitol and arabinitol, the preferential alignment of HBs along the x- and z-axis directions matched the directions of higher TC in this work. In the liquid phase, HB orientation distributions are nearly uniform, aligning with the observed isotropy in TC. The results emphasized the critical role of hydrogen bonding networks in facilitating efficient heat transfer, especially in the solid phase.

Overall, this study provides a molecular-level understanding of how temperature, phase state, molecular structure, and hydrogen bonding collectively govern the thermal conductivity behavior of sugar alcohols. Highlights that anisotropic TC can be effectively engineered by deliberately selecting crystal structures and strategically positioning hydroxyl groups to align HBs along desired directions. Such control over HB alignment opens promising avenues for tailoring TC in materials, particularly in applications where directional heat transfer is advantageous, such as thermal interface materials or PCMs in thermal management systems. Additionally, our results emphasize that while HBs play a crucial role, they are not the sole contributors to TC, other molecular interactions must also be considered to fully understand and optimize heat conduction behavior. Importantly, the strong agreement between our MD simulation results and experimental thermal conductivities underscores the potential of MD as a predictive and efficient tool for the preliminary design and screening of PCM candidates.

CRediT authorship contribution statement

Shukai Cheng: Writing – review & editing, Writing – original draft, Visualization, Software, Methodology, Investigation, Data curation, Conceptualization. **Donatas Surblys:** Writing – review & editing, Software, Methodology, Conceptualization. **Taku Ohara:** Writing – review & editing, Project administration, Conceptualization.

Declaration of competing interest

The authors declare that they have no known competing financial interests or personal relationships that could have appeared to influence the work reported in this paper.

Acknowledgment

This work was supported by JSPS Kakenhi, JP24K00815. The computational simulations were performed on the Supercomputer system “AFI-NITY” at the Advanced Fluid Information Research Center, Institute of Fluid Science, Tohoku University.

Supplementary materials

Supplementary material associated with this article can be found, in the online version, at doi:10.1016/j.ijheatmasstransfer.2025.127709.

Data availability

Data will be made available on request.

References

[1] A. Anand, M. Mansor, K. Sharma, A. Shukla, A. Sharma, M.I.H. Siddiqui, K. K. Sadasivuni, N. Priyadarshi, B. Twala, A comprehensive review on eutectic phase change materials: development, thermophysical properties, thermal stability, reliability, and applications, Alex. Eng. J. 112 (2025) 254–280, https://doi.org/10.1016/j.aej.2024.10.054.

[2] F. Odoi-Yorke, J.E. Davis, R. Nyarkoh, A.A. Abbey, E.B. Agyekum, F.P. Lamptey, G. S. Otoo, S.A. Kaburi, R.O. Darko, L. Atepor, A review of research trends, innovations, and future directions in phase change materials for energy storage in solar drying systems: a bibliometric approach, J. Energy Storage 118 (2025) 116233, https://doi.org/10.1016/j.est.2025.116233.

[3] C. Hong, J. Chai, Z. Li, X. Kong, B. Xu, Experimental study on binary phase change material with excellent supercooled stability and superior thermal physical properties for seasonal heat storage, J. Energy Storage 117 (2025) 116224, https://doi.org/10.1016/j.est.2025.116224.

[4] J. Luo, D. Zou, Y. Wang, S. Wang, L. Huang, Battery thermal management systems (BTMs) based on phase change material (PCM): a comprehensive review, Chem. Eng. J. 430 (2022) 132741, https://doi.org/10.1016/j.cej.2021.132741.

[5] R. Loni, G. Najafi, E. Bellos, F. Rajaee, Z. Said, M. Mazlan, A review of industrial waste heat recovery system for power generation with Organic Rankine cycle: recent challenges and future outlook, J. Clean. Prod. 287 (2021) 125070, https://doi.org/10.1016/j.jclepro.2020.125070.

[6] W. Lee, J. Kim, A comprehensive review of research on organic-based phase-change thermal interface materials for thermal management of electric devices: methods, performance, and applications, Polym. Test. 142 (2025) 108677, https://doi.org/10.1016/j.polymertesting.2024.108677.

[7] S.A. Mohamed, F.A. Al-Sulaiman, N.I. Ibrahim, Md.H. Zahir, A. Al-Ahmed, R. Saidur, B.S. Yılbaş, A.Z. Sahin, A review on current status and challenges of inorganic phase change materials for thermal energy storage systems, Renew. Sustain. Energy Rev. 70 (2017) 1072–1089, https://doi.org/10.1016/j.rser.2016.12.012.

[8] E. Palomo Del Barrio, R. Cadoret, J. Daranlot, F. Achchaq, New sugar alcohols mixtures for long-term thermal energy storage applications at temperatures between 70°C and 100°C, Sol. Energy Mater. Sol. Cells 155 (2016) 454–468, https://doi.org/10.1016/j.solmat.2016.06.048.

[9] T. Inagaki, T. Ishida, Computational design of non-natural sugar alcohols to increase thermal storage density: beyond existing organic phase change materials, J. Am. Chem. Soc. 138 (2016) 11810–11819, https://doi.org/10.1021/jacs.6b05902.

[10] S. Cheng, D. Surblys, T. Ohara, Molecular dynamics study on phase change properties and their nano-mechanism of sugar alcohols: melting and latent heat, Int. J. Heat Mass Transf. 234 (2024) 126104, https://doi.org/10.1016/j.ijheatmasstransfer.2024.126104.

[11] A. Ribezzo, G. Falciani, L. Bergamasco, M. Fasano, E. Chiavazzo, An overview on the use of additives and preparation procedure in phase change materials for thermal energy storage with a focus on long term applications, J. Energy Storage 53 (2022) 105140, https://doi.org/10.1016/j.est.2022.105140.

[12] S. Salyan, S. Suresh, Study of thermo-physical properties and cycling stability of D-Mannitol-copper oxide nanocomposites as phase change materials, J. Energy Storage 15 (2018) 245–255, https://doi.org/10.1016/j.est.2017.10.013.

[13] S. Salyan, S. Suresh, Multi-walled carbon nanotube laden with D-Mannitol as phase change material: characterization and experimental investigation, Adv. Powder Technol. 29 (2018) 3183–3191, https://doi.org/10.1016/j.apt.2018.08.021.

[14] L. Gao, J. Zhao, Q. An, D. Zhao, F. Meng, X. Liu, Experiments on thermal performance of erythritol/expanded graphite in a direct contact thermal energy storage container, Appl. Therm. Eng. 113 (2017) 858–866, https://doi.org/10.1016/j.applthermaleng.2016.11.073.

[15] X. Qin, N. Feng, Z. Kang, D. Hu, Construction of wood-based cellulose micro-framework composite form-stable multifunctional materials with thermal and electrical response via incorporating erythritol-urea (thiourea)-carbon nanotubes, Int. J. Biol. Macromol. 184 (2021) 538–550, https://doi.org/10.1016/j.ijbiomac.2021.06.150.

[16] A. Ghavipanjeh, S. Sadeghzadeh, Tailoring the thermal transport properties of cellulose and lignin laser-induced graphene, Comput. Mater. Sci. 244 (2024) 113240, https://doi.org/10.1016/j.commatsci.2024.113240.

[17] A. Ghavipanjeh, S. Sadeghzadeh, Diffusion properties of silk-derived laser-induced graphene, Diam. Relat. Mater. 146 (2024) 111172, https://doi.org/10.1016/j.diamond.2024.111172.

[18] H. Tafrishi, S. Sadeghzadeh, R. Ahmadi, Molecular dynamics simulations of phase change materials for thermal energy storage: a review, RSC Adv 12 (2022) 14776–14807, https://doi.org/10.1039/D2RA02183H.

[19] T. Ohara, Intermolecular energy transfer in liquid water and its contribution to heat conduction: a molecular dynamics study, J. Chem. Phys. 111 (1999) 6492–6500, https://doi.org/10.1063/1.480025.

[20] L.S. Dodda, I. Cabeza de Vaca, J. Tirado-Rives, W.L. Jorgensen, LigParGen web server: an automatic OPLS-AA parameter generator for organic ligands, Nucleic Acids Res 45 (2017) W331–W336, https://doi.org/10.1093/nar/gkx312.

[21] R.W. Hockney, J.W. Eastwood, Computer Simulation Using Particles, CRC Press, Boca Raton, 2021, https://doi.org/10.1201/9780367806934.

[22] H.C. Andersen, Rattle: a "velocity" version of the shake algorithm for molecular dynamics calculations, J. Comput. Phys. 52 (1983) 24–34, https://doi.org/10.1016/0021-9991(83)90014-1.

[23] J. Wouters, L. Van Meervelt, Classroom experiments with artificial sweeteners: growing single crystals and simple calorimetry, Acta Crystallogr. Sect. E Crystallogr. Commun. 78 (2022) 874–879, https://doi.org/10.1107/S2056989022007617.

[24] T. Kusukawa, G. Niwa, T. Sasaki, R. Oosawa, W. Himeno, M. Kato, Observation of a hydrogen-bonded 3D structure of crystalline glycerol, Bull. Chem. Soc. Jpn. 86 (2013) 351–353, https://doi.org/10.1246/bcsj.20120300.

[25] P. Derollez, Y. Guinet, F. Affouard, F. Danède, L. Carpentier, A. Hédoux, Structure determination of L-arabinitol by powder X-ray diffraction, Acta Crystallogr. B 68 (2012) 407–411, https://doi.org/10.1107/S0108768112019994.

[26] F.R. Fronczek, H.N. Kamel, M. Slattery, Three polymorphs (α, β, and δ) of D-mannitol at 100 K, Acta Crystallogr. C 59 (2003) o567–o570, https://doi.org/10.1107/S0108270103018961.

[27] L. Verlet, Computer "experiments" on classical fluids. I. Thermodynamical properties of Lennard-Jones molecules, Phys. Rev. 159 (1967) 98–103, https://doi.org/10.1103/PhysRev.159.98.

[28] A.P. Thompson, H.M. Aktulga, R. Berger, D.S. Bolintineanu, W.M. Brown, P. S. Crozier, P.J. in 't Veld, A. Kohlmeyer, S.G. Moore, T.D. Nguyen, R. Shan, M. J. Stevens, J. Tranchida, C. Trott, S.J. Plimpton, LAMMPS - a flexible simulation tool for particle-based materials modeling at the atomic, meso, and continuum scales, Comput. Phys. Commun. 271 (2022) 108171, https://doi.org/10.1016/j.cpc.2021.108171.

[29] W. Humphrey, A. Dalke, K. Schulten, VMD: visual molecular dynamics, J. Mol. Graph. 14 (1996) 33–38, https://doi.org/10.1016/0263-7855(96)00018-5.

[30] W.G. Hoover, Canonical dynamics: equilibrium phase-space distributions, Phys. Rev. A 31 (1985) 1695–1697, https://doi.org/10.1103/PhysRevA.31.1695.

[31] H. Matsubara, G. Kikugawa, M. Ishikiriyama, S. Yamashita, T. Ohara, Equivalence of the EMD- and NEMD-based decomposition of thermal conductivity into microscopic building blocks, J. Chem. Phys. 147 (2017) 114104, https://doi.org/10.1063/1.4990593.

[32] R. Kubo, The fluctuation-dissipation theorem, Rep. Prog. Phys. 29 (1966) 255, https://doi.org/10.1088/0034-4885/29/1/306.

[33] H. Matsubara, T. Ohara, Effect of the in-plane aspect ratio of a graphene filler on anisotropic heat conduction in paraffin/graphene composites, Phys. Chem. Chem. Phys. 23 (2021) 12082–12092, https://doi.org/10.1039/D1CP00556A.

[34] R. Berman, Heat conduction in non-metallic crystals, Sci. Prog. 1933-55 (1967) 357–377.

[35] D. Bolmatov, The Phonon Theory of liquids and biological fluids: developments and applications, J. Phys. Chem. Lett. 13 (2022) 7121–7129, https://doi.org/10.1021/acs.jpclett.2c01779.

[36] H. Sun, D. Surblys, H. Matsubara, T. Ohara, Molecular dynamics study on the role of hydrogen bonds and interfacial heat transfer between diverse silica surfaces and organic liquids, Int. J. Heat Mass Transf. 208 (2023) 124091, https://doi.org/10.1016/j.ijheatmasstransfer.2023.124091.

[37] H. Matsubara, D. Surblys, Y. Bao, T. Ohara, Molecular dynamics study on vibration-mode matching in surfactant-mediated thermal transport at solid–liquid interfaces, J. Mol. Liq. 347 (2022) 118363, https://doi.org/10.1016/j.molliq.2021.118363.

[38] A. Seppälä, K. Turunen, M.R. Yazdani, Thermal conductivity of sugar alcohols, Sol. Energy Mater. Sol. Cells 243 (2022) 111796, https://doi.org/10.1016/j.solmat.2022.111796.

[39] O. Andersson, G.P. Johari, Thermal conductivity of Glycerol's liquid, glass, and crystal states, glass-liquid-glass transition, and crystallization at high pressures, J. Chem. Phys. 144 (2016) 064504, https://doi.org/10.1063/1.4941335.

[40] J. Fan, S. Liu, C. Gao, F. Song, Molecular dynamic simulation on the transport properties of alcohols, Case Stud. Therm. Eng. 32 (2022) 101888, https://doi.org/10.1016/j.csite.2022.101888.

[41] C.A. Brookes, J.B. O'Neill, B.a.W. Redfern, D. Tabor, Anisotropy in the hardness of single crystals, Proc. R. Soc. Lond. Math. Phys. Sci. 322 (1997) 73–88, https://doi.org/10.1098/rspa.1971.0055.

[42] J.-W. Handgraaf, E.J. Meijer, M.-P. Gaigeot, Density-functional theory-based molecular simulation study of liquid methanol, J. Chem. Phys. 121 (2004) 10111–10119, https://doi.org/10.1063/1.1809595.

[43] Y. Zhao, G. Kikugawa, Y. Kawagoe, K. Shirasu, T. Okabe, Molecular-scale investigation on relationship between thermal conductivity and the structure of crosslinked epoxy resin, Int. J. Heat Mass Transf. 198 (2022) 123429, https://doi.org/10.1016/j.ijheatmasstransfer.2022.123429.

[44] A.R. Ubbelohde, Melting and crystal structure, Q. Rev. Chem. Soc. 4 (1950) 356–381, https://doi.org/10.1039/QR9500400356.

[45] P. Carruthers, Theory of thermal conductivity of solids at low temperatures, Rev. Mod. Phys. 33 (1961) 92–138, https://doi.org/10.1103/RevModPhys.33.92.

[46] R.J. Gowers, M. Linke, J. Barnoud, T.J.E. Reddy, M.N. Melo, S.L. Seyler, J. Domański, D.L. Dotson, S. Buchoux, I.M. Kenney, O. Beckstein, MDAnalysis: a Python package for the rapid analysis of molecular dynamics simulations, in: Proc. 15th Python Sci. Conf., 2016, pp. 98–105, https://doi.org/10.25080/Majora-629e541a-00e.

[47] T.I. Mizan, P.E. Savage, R.M. Ziff, Temperature dependence of hydrogen bonding in supercritical water, J. Phys. Chem. 100 (1996) 403–408, https://doi.org/10.1021/jp951561t.

[48] M.P. Alferez Luna, H. Neumann, S. Gschwander, Stability study of erythritol as phase change material for medium temperature thermal applications, Appl. Sci. 11 (2021) 5448, https://doi.org/10.3390/app11125448.

[49] E. Parzen, On estimation of a probability density function and mode, Ann. Math. Stat. 33 (1962) 1065–1076.

[50] R. Cao, A. Cuevas, W. González Manteiga, A comparative study of several smoothing methods in density estimation, Comput. Stat. Data Anal. 17 (1994) 153–176, https://doi.org/10.1016/0167-9473(92)00066-Z.